

## Thermally quenched metastable phase in the Ising model with competing interactions

Hiroshi Oike <sup>1,2,\*</sup>, Hidemaro Suwa <sup>3</sup>, Yasunori Takahashi,<sup>4</sup> and Fumitaka Kagawa <sup>5,6</sup>

<sup>1</sup>*PRESTO, Japan Science and Technology Agency (JST), Saitama 332-0012, Japan*

<sup>2</sup>*Research Center for Materials Nanoarchitectonics (MANA), National Institute for Materials Science (NIMS), Ibaraki 305-0047, Japan*

<sup>3</sup>*Department of Physics, The University of Tokyo, Tokyo 113-0033, Japan*

<sup>4</sup>*Department of Applied Physics and Quantum-Phase Electronics Centre (QPEC), The University of Tokyo, Tokyo 113-8656, Japan*

<sup>5</sup>*Department of Physics, Institute of Science Tokyo, Meguro 152-8551, Japan*

<sup>6</sup>*RIKEN Center for Emergent Matter Science (CEMS), Wako 351-0198, Japan*



(Received 16 April 2025; revised 2 July 2025; accepted 9 July 2025; published 6 August 2025)

Thermal quenching has been employed to discover various metastable materials such as hard steels and metallic glasses. More recently, quenching-based phase control has been applied to correlated electron systems that exhibit metal-insulator, magnetic, or superconducting transitions. Despite the discovery of metastable electronic phases, however, the microscopic origin of metastability remains elusive, as the system's degrees of freedom—such as electrons—can vary even at low temperatures. Here, using Monte Carlo simulations, we demonstrate a thermally quenched metastable phase in the Ising model that does not conserve the total magnetization. When multiple types of interactions that stabilize different long-range orders are introduced, the ordering kinetics exhibits significant slowing down, and the characteristic timescale for ordering diverges as the temperature decreases. As a result, the system can reach low temperatures without undergoing ordering if the cooling rate is sufficiently high. Quantitative analysis of the divergent behavior suggests that the energy barrier for eliminating the local structure of competing orders is the origin of this metastability. Thus, the present simulation demonstrates that competing interactions play an essential role in achieving metastability.

DOI: [10.1103/ycd4-cfrm](https://doi.org/10.1103/ycd4-cfrm)

### I. INTRODUCTION

The thermodynamically most stable phase of a material is uniquely determined when thermodynamic parameters such as the temperature, pressure, and chemical composition are fixed. In contrast, multiple metastable phases may exist for a given thermodynamic parameter. For example, although an aggregate of carbon atoms has graphite as the most stable phase under ambient conditions, several allotropes, such as diamond and lonsdaleite, exist as metastable phases [1]. Using metastable phases as an exploration space, solid-state chemistry and metallurgy have been developed [2–6]. A metastable phase is often achieved via thermal quenching, as exemplified by the glassy state that occurs when a liquid is cooled so rapidly that crystallization is kinetically avoided [7–10]. More recently, quenching-based phase control has been applied to correlated electron materials, realizing metastable electronic phases such as charge glasses [11–13], charge density waves [14], magnetic skyrmions [15–18], orbital disordered phases [19], ferromagnetic phases [20,21], and superconductivity [22]. Furthermore, the metastable phase of correlated elec-

trons is also realized through intense excitation of electrons using pulsed lasers [23,24]. Thus, metastability is becoming a widely researched topic in materials science.

Along with the development of methods for making glasses, their design principles have also been clarified. Supercooled liquids tend to have a high glass forming ability near a eutectic point [Fig. 1(a)], as exemplified by molten alloys [8], pressurized silicon [25], and salt-added water [26]. The microscopic mechanism underlying this behavior has been investigated [27–29]. A similar guiding principle may be applied to metastable electronic phases. However, this principle is not straightforward because crystallization differs from metal-insulator transitions or magnetic phase transitions in terms of the dynamics of the microscopic components. Atomic diffusion often divergently slows at low temperatures according to the Vogel-Fischer law [30], resulting in metastabilization of the supercooled liquid. In contrast, in metal-insulator transitions and magnetic phase transitions, the internal degrees of freedom of the electrons can vary to minimize the free energy of the electronic system even at low temperatures. Therefore, a thermally quenched electronic phase may not be metastable.

The present study aims to generalize the dynamics and metastable states near a eutectic-like triple point. The Ising model is suitable for this purpose because it is a typical statistical mechanics model for describing phase transitions involving the rearrangement of atoms [31,32] and the internal degrees of freedom of electrons [33,34]. When eutectic crystallization is modeled with the Ising model, one element

\*Contact author: [oike.hiroshi@nims.go.jp](mailto:oike.hiroshi@nims.go.jp)

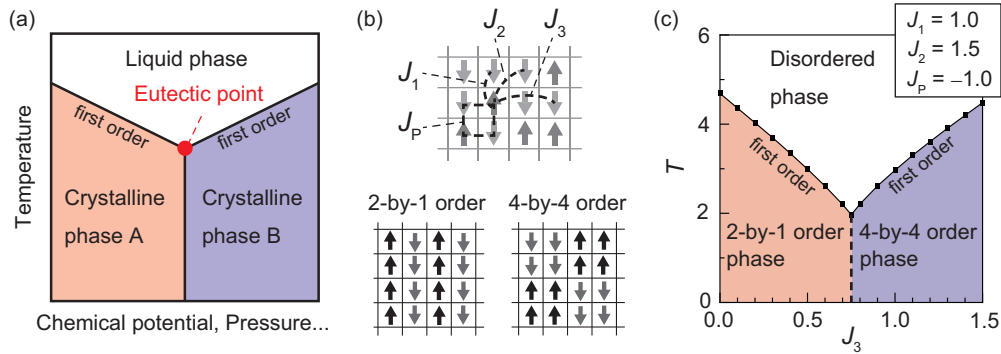


FIG. 1. (a) Typical eutectic phase diagram. (b) Schematic diagram of the interactions between spins in the Ising model and the ordered phases of interest. (c)  $T$ - $J_3$  phase diagram where  $J_1$ ,  $J_2$ , and  $J_p$  are fixed to 1.0, 1.5, and  $-1.0$ , respectively. Since almost all crystallization processes are first-order phase transitions, the parameters were set so that the ordered phase would also be formed by a first-order phase transition (see Appendix A). A eutecticlike triple point exists at parameters of  $(T, J_3) = (2.0, 0.75)$ .

is mapped to the up spin and another to the down spin. The conservation of the number of atoms corresponds to the conservation of magnetization, which is defined by the difference in the numbers of up and down spins. This conservation law imposes constraints on changes in the spin configuration, resulting in energy barriers in the process corresponding to the exchange of atoms and the movement of an atom into a vacancy [35,36]. In contrast to eutectic crystallization, the conservation laws are sometimes broken in correlated electron systems, such as in the phase transition from paramagnetic to ferromagnetic phases. Therefore, in the present study, our focus is on the nonconserved Ising model, in which the spin of each site can change independently. The pioneering works clarified the metastability in the phase transition between ordered phases [37,38] and the metastability of a supercooled disordered phase in the Ising model with plaquette interactions [39–42], but the metastability of the disordered phase near a eutectic-like triple point has not been clarified. Nevertheless, we find that a thermally quenched disordered phase exhibits metastability near the eutecticlike triple point in the Ising model with competing interactions that favor different ordered structures. This result suggests that the design principles for glass are also applicable to correlated electron systems.

The remainder of this paper is organized as follows. Section II describes the simulation method. In Sec. III, we present the emergence of a metastable phase, followed by the temperature-dependent ordering kinetics of the system in Sec. IV. In Sec. V, we discuss the ordering kinetics and structural factors to explore the relationship between the energy competition of two ordered phases and the metastability of a disordered phase. Section VI discusses the implications of our results for metastable materials and strongly correlated electron systems. Finally, Sec. VII provides concluding remarks.

## II. SIMULATION METHOD

To implement a eutecticlike triple point in the phase diagram of the Ising model, we consider a two-dimensional square lattice and introduce the Hamiltonian with several

types of interactions following a previous study [43]:

$$H = J_1 \sum_{n,n} \sigma_i \sigma_j + J_2 \sum_{2nd} \sigma_i \sigma_j + J_3 \sum_{3rd} \sigma_i \sigma_j + J_p \sum_{ring} \sigma_i \sigma_j \sigma_k \sigma_l, \quad (1)$$

where  $J_1$ ,  $J_2$ ,  $J_3$ , and  $J_p$  are the nearest-neighbor, next-nearest neighbor, third-nearest neighbor, and four-body ring interactions, respectively, as shown in Fig. 1(b).  $\sigma_i$  represents a spin, which indicates the local configuration at lattice site  $i$  and takes a value of  $+1$  or  $-1$ .  $J_1$  favors a checkerboard antiferromagnetic order,  $J_2$  favors a 2-by-1 order, and  $J_3$  favors a 4-by-4 order.  $J_p$  represents the many-body spin interactions arising from higher-order effects of electron itinerancy [44,45] and contributes to the ordering temperature and discontinuity of the phase transition. When the interaction parameters ( $J_1$ ,  $J_2$ ,  $J_p$ ) are fixed to (1.0, 1.5,  $-1.0$ ), the most stable ordered phase changes from a 2-by-1 order to a 4-by-4 order with variation of  $J_3$ , as shown in Fig. 1(c). The disordered, 2-by-1, and 4-by-4 phases meet at the parameters of  $(T, J_3) = (2.0, 0.75)$ , which is a eutectic-like triple point. Thus, our simple Hamiltonian successfully realizes a phase diagram with a eutecticlike triple point.

The isothermal phase transition kinetics are then simulated at each point of the  $T$ - $J_3$  phase diagram. The  $\sigma_i$  values in an initial state are randomly set to 1 or  $-1$  to simulate a state immediately after thermal quenching from an infinite temperature with an infinite cooling rate. The time evolution of  $\sigma_i$  is simulated by the single spin-flip and heat-bath methods, in which the values of  $\sigma_i$  are updated after a Monte Carlo step with the probabilities

$$P(\sigma_i = 1) = \frac{\exp[-H(\sigma_i = 1)/T]}{Z}, \quad (2)$$

$$P(\sigma_i = -1) = \frac{\exp[-H(\sigma_i = -1)/T]}{Z}, \quad (3)$$

$$Z = \exp[-H(\sigma_i = 1)/T] + \exp[-H(\sigma_i = -1)/T]. \quad (4)$$

During one Monte Carlo step, all the sites are updated in a random order. In this study, a Monte Carlo step was considered a unit of time, as in previous studies [38,46,47]. We imposed periodic boundaries and performed simulations and analyses. In the main text, we present the results for a system

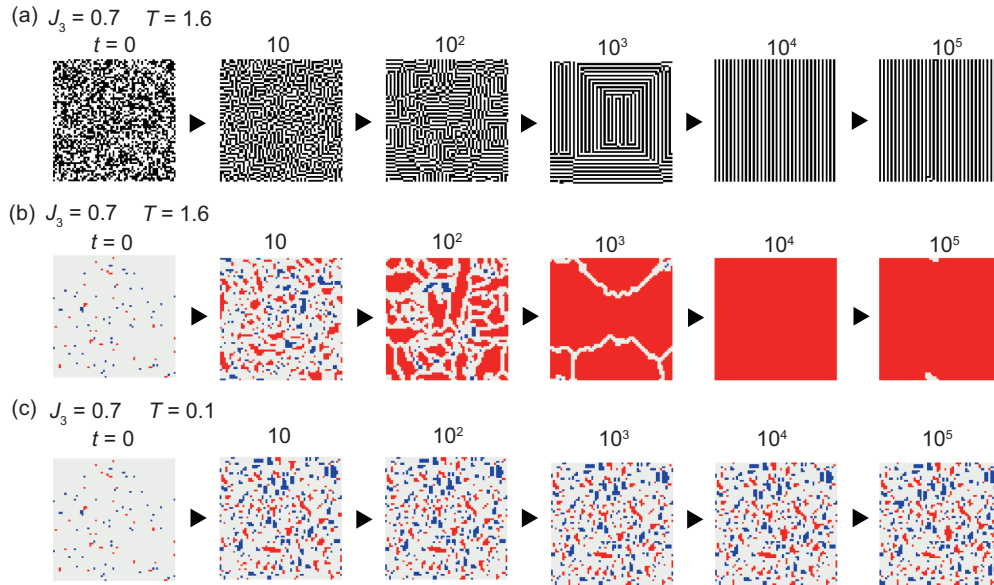


FIG. 2. (a) Isothermal time evolution of the spin configuration at parameters of  $(T, J_3) = (1.6, 0.7)$ . The system size  $N$  is  $64^2$ . (b) Three-colored representation of the time evolution shown in panel (a). (c) Three-colored representation of the time evolution at parameters of  $(T, J_3) = (0.1, 0.7)$ . The red and blue areas represent 2-by-1 and 4-by-4 orders, respectively, and the white area represents all other configurations. The method of converting the spin configurations to three colors is described in the main text.

size  $N$  of  $64^2$ , which is large enough to study the fundamental properties, as discussed in Appendix B.

### III. EMERGENCE OF METASTABILITY

To examine metastability, the isothermal time evolution is studied for the parameters of  $(T, J_3) = (1.6, 0.7)$  and  $(0.1, 0.7)$ , where  $J_3$  is slightly decreased from the critical value of the eutectic point, 0.75, so that the 2-by-1 order becomes the most stable phase. At a temperature of  $T = 1.6$ , stripe-structured domains representing the 2-by-1 order appear, and the domains gradually increase in size, becoming a uniform 2-by-1 order as time evolves [Fig. 2(a)]. To make the phase transition process with time easier to understand, the three types of local structures (2-by-1 order, 4-by-4 order, and disordered) are colored differently according to the following procedure. First, a site is selected, and 3-by-3 sites containing the selected site at the center are extracted. The selected site is colored red if the 3-by-3 sites match the 2-by-1 order, colored blue if they match the 4-by-4 order, or colored white if they do not match either of these orders. Thus, many small 2-by-1 and 4-by-4-order domains appear in the initial stage, and the 2-by-1 domains coarsen over time until they become comparable to the system size [Fig. 2(b)]. The ordering kinetics from the supercooled disordered phase presented below were obtained through this procedure.

In contrast to that at  $T = 1.6$ , the real-space configuration at  $T = 0.1$  is approximately independent of time from  $t = 10$  to  $t = 10^5$  [Fig. 2(c)]. This time-independent behavior means that the disordered phase is stable on the timescale of the simulation. This disordered phase is considered metastable because the free-energetically most stable phase is a uniform 2-by-1 order. The comparison of the configurations at  $t = 0$  and  $t = 10^5$  indicates that the metastable phase is not a random state of the initial state but a fine domain structure of

2-by-1 and 4-by-4 orders. The formation of a fine structure suggests that local energy optimization occurs in the early stages but that global optimization has not yet occurred.

### IV. TIME-TEMPERATURE-TRANSFORMATION (TTT) DIAGRAM

To obtain an overview of the temperature dependence, we examine the TTT diagram at  $J_3 = 0.7$ , as thermally quenched metastable phases are often discussed using the TTT diagram [7, 13, 48], which summarizes the temperature-dependent isothermal time evolution of an order parameter. To characterize the extent to which the ordering progresses, we define the order parameters for the 2-by-1 and 4-by-4 phases as follows:

$$\phi(2\text{by}1) = \frac{1}{N} \sqrt{\sum_{q=q_x, q_y} \left| \sum_{j=1}^N \sigma_j e^{iq \cdot r_j} \right|^2}, \quad (5)$$

$$\phi(4\text{by}4) = \frac{1}{N} \sqrt{\sum_{q=q_p, q_m, -q_p, -q_m} \left| \sum_{j=1}^N \sigma_j e^{iq \cdot r_j} \right|^2}, \quad (6)$$

where  $N$  is the number of sites and  $q_x$ ,  $q_y$ ,  $q_p$ , and  $q_m$  are  $(\pi, 0)$ ,  $(0, \pi)$ ,  $(\pi/2, \pi/2)$ , and  $(\pi/2, -\pi/2)$ , respectively. These definitions lead to  $\phi(2\text{by}1)$  and  $\phi(4\text{by}4)$  being equal to 1 in the uniformly ordered states and approximately 0 in an initial state with a random configuration. The isothermal time evolution for several temperatures is obtained by averaging 64 individual runs, as shown in Fig. 3(a). By making a contour map of the time evolution of  $\phi(2\text{by}1)$  up to  $t = 10^5$  for  $T = 0.001, 0.2, 0.4, 0.6, 0.8, 1, 1.2, 1.4, 1.6, 1.8, 2.0$ , and 2.2, a TTT diagram is obtained, as shown in Fig. 3(b).

As shown in Fig. 3(b),  $\phi(2\text{by}1)$  rapidly develops over time within a temperature range of  $1.5 < T < 2.0$ , whereas its evolution dynamics slow at higher and lower temperatures.

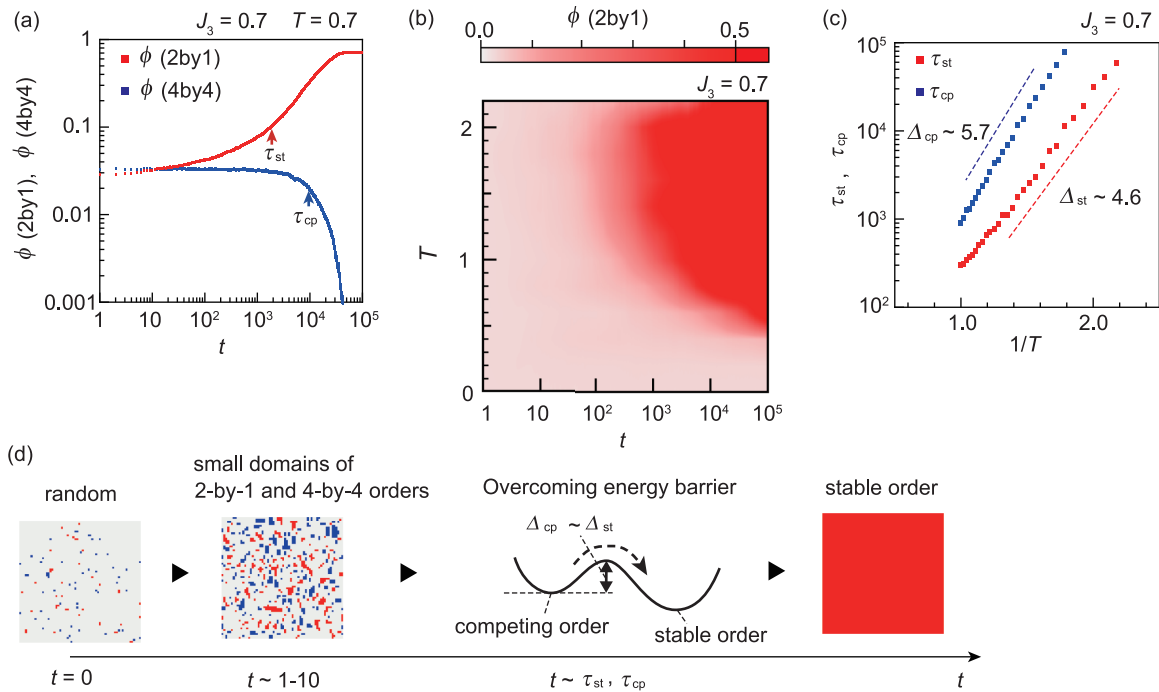


FIG. 3. (a) Isothermal time evolution of order parameters  $\phi(2by1)$  and  $\phi(4by4)$  at parameters of  $(T, J_3) = (0.7, 0.7)$ .  $\tau_{st}$  and  $\tau_{cp}$  represent the times at which the order parameter of the stable order exceeds 0.1 and that the order parameter of the competing order decreases to half its value at  $t = 1$ , respectively. The stable order is a 2-by-1 order for  $J_3$  less than 0.75 and a 4-by-4 order for  $J_3$  greater than 0.75, with the competing order being the opposite. (b) TTT diagram of the Ising model at a  $J_3$  of 0.7. (c) Arrhenius plot of the growth time of the stable 2-by-1 order  $\tau_{st}$  and the destruction time of the competing 4-by-4 order  $\tau_{cp}$ .  $\Delta_{st}$  and  $\Delta_{cp}$  were extracted from the slopes of the Arrhenius plots of  $\tau_{st}$  and  $\tau_{cp}$ , respectively. (d) Schematic representation of the time evolution. From the initial random arrangement, fine 2-by-1 and 4-by-4 domains rapidly form, and when the process of overcoming the energy barrier  $\Delta_{st}$ , which is comparable to  $\Delta_{cp}$ , is activated by thermal fluctuations, a uniform 2-by-1 order is formed.

In particular, within a temperature range of  $T < 0.4$ , the ordering hardly progresses, and the system does not reach the most stable 2-by-1 phase, at least within the timescale of the simulation, indicating the emergence of metastability. This nonmonotonic temperature dependence is commonly observed in supercooled liquids and arises from two competing temperature dependencies: the energy barriers in the phase transition pathway are less likely to be overcome at low temperatures, whereas the free-energy driving force for ordering becomes greater at low temperatures. The TTT diagram for the present Ising model suggests the existence of an energy barrier.

To characterize the timescale over which a stable ordered phase is formed, we define  $\tau_{st}$  as the time at which the order parameter of the stable order exceeds 0.1. The examination of  $\tau_{st}$  at various temperatures reveals that  $\tau_{st}$  follows an Arrhenius-type behavior [Fig. 3(c)], indicating the presence of a thermal activation barrier  $\Delta_{st}$  [Fig. 3(d)]. For supercooled liquids, the diffusion of atoms is widely believed to contribute to the energy barrier [35,36]. However, note that a finite  $\Delta_{st}$  appears, although individual degrees of freedom are variable without a diffusion process in the present nonconserved system.

To gain insight into the energy barrier, the dynamics of the disappearing competing order are characterized by the time  $\tau_{cp}$  at which  $\phi(4by4)$  is half of the value at  $t = 1$ . The examination of  $\tau_{cp}$  at various temperatures reveals that  $\tau_{cp}$  also shows an Arrhenius-type temperature dependence with

a thermal activation barrier  $\Delta_{cp}$  [Fig. 3(c)]. A possible reason for the close values of  $\Delta_{st}$  and  $\Delta_{cp}$  is that the rate-limiting process of the phase transition is breaking competing orders.

## V. ENERGETIC COMPETITION AND METASTABILITY

Because  $J_3$  controls the relative stability of the 2-by-1 and 4-by-4 orders, we then examine the  $J_3$  dependence of the phase transition kinetics and metastability. To overview the  $J_3$  dependence, the values of  $\phi(2by1) - \phi(4by4)$  are plotted in Fig. 4(a) as contour maps in the  $J_3$ - $T$  plane at  $t = 1, 10, 10^2, 10^3, 10^4, 10^5$ . As the 2-by-1 (4-by-4) order grows, the red (blue) color becomes clearer in the contour maps [Fig. 4(a)]. At a  $J_3$  close to 0 or 1.5, the ordering appreciably progresses at  $t = 10$  and is almost complete at  $t = 10^3$ . As  $J_3$  becomes closer to that at the eutecticlike point ( $J_3 = 0.75$ ), both  $\phi(2by1)$  and  $\phi(4by4)$  remain at values less than 0.1 even at  $t = 10^5$  within a temperature range of  $T < 0.5$ .

To characterize the region in which the metastable phases exist in the  $J_3$ - $T$  phase diagram, we define the upper temperature limit of metastability  $T_m$  as the temperature below which  $\phi(2by1)$  and  $\phi(4by4)$  are less than 0.1 at  $t = 10^5$ , and the  $J_3$  dependence of  $T_m$  is also plotted in the  $J_3$ - $T$  phase diagram at  $t = 10^5$  [Fig. 4(a)].  $T_m$  is found to take a maximum value near  $J_3 = 0.75$ , indicating that the system tends to be metastable near the phase boundary between the 2-by-1 and 4-by-4 phases. The energy barriers  $\Delta_{st}$  and  $\Delta_{cp}$  also take a maximum near  $J_3 = 0.75$  [Fig. 4(b)] and are positively correlated with

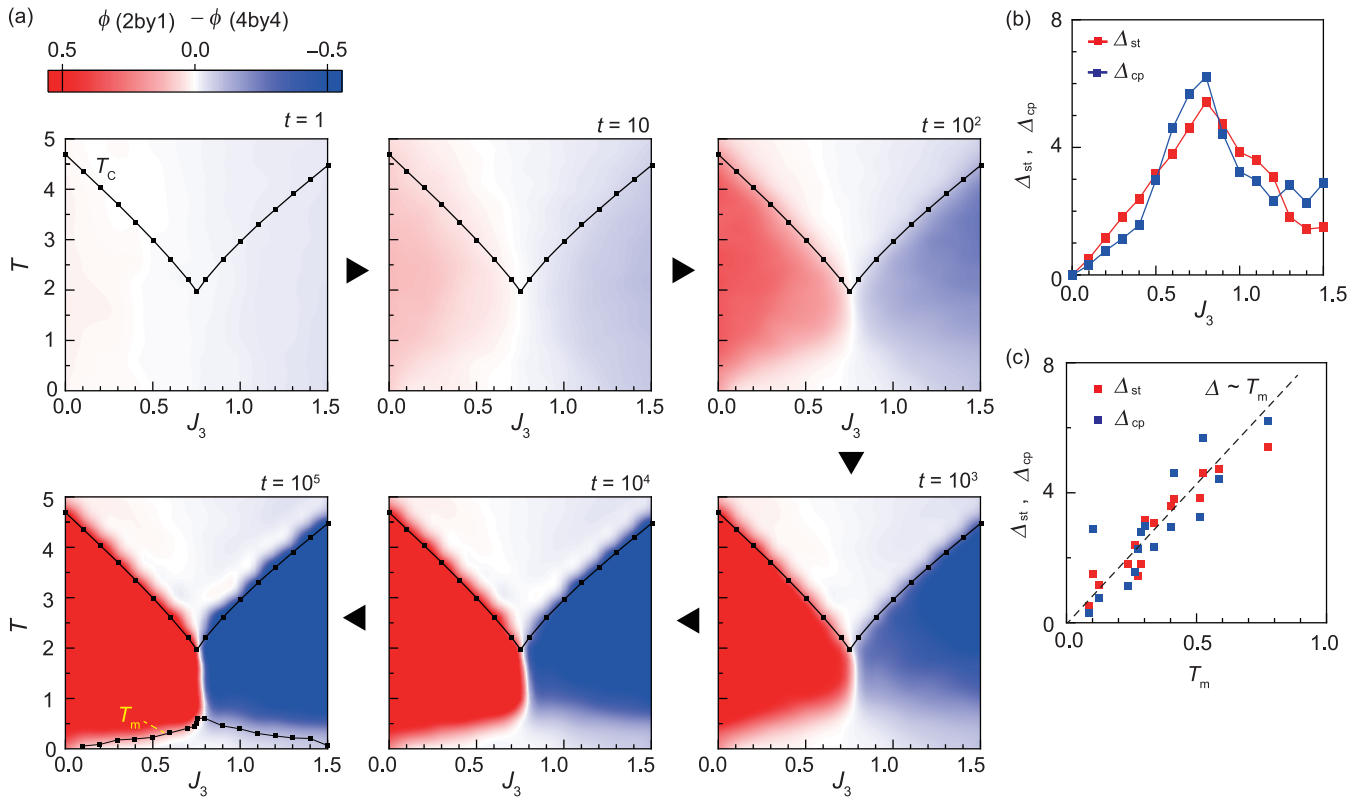


FIG. 4. (a) Contour plot of the time evolution of the order parameter in the  $J_3$  range of 0–1.5.  $\phi(2\text{by}1) - \phi(4\text{by}4)$  is plotted, as the formation of the 2-by-1 order is indicated by a positive value (red) and the formation of the 4-by-4 order is indicated by a negative value (blue).  $T_m$  is the temperature below which  $\phi(2\text{by}1)$  or  $\phi(4\text{by}4)$  is less than 0.1 at  $t = 10^5$ . (b)  $J_3$  dependence of the energy barriers  $\Delta_{st}$  and  $\Delta_{cp}$  estimated with the Arrhenius plot shown in Fig. 3(c). (c) Correlations between  $T_m$  and the energy barriers  $\Delta_{st}$  and  $\Delta_{cp}$ . A guide to the eye is used to show the proportional relationship.

$T_m$  [Fig. 4(c)]. Thus, the  $J_3$ -dependent energy barrier is found to play a key role in controlling the metastability in our model system with a eutecticlike triple point.

The good correspondence between the evolution of the energy barriers and that of the metastability suggests that the local configuration is correlated with the metastability. To address this issue in more detail, below we examine the disordered metastable state in terms of the structure factor. At a temperature of  $T = 0.1$  and  $J_3$  values of 0.4, 0.7, 0.8, and 1.1, the metastable disordered phases contain both 2-by-1 and 4-by-4 domains, the fractions of which depend on  $J_3$  [Figs. 5(a)–5(d)]. To quantify the domain fractions, the real-space configurations are converted into the structure factor  $S(\mathbf{q})$  as

$$S(\mathbf{q}) = \frac{1}{N} \left| \sum_{j=1}^N \sigma_j e^{i\mathbf{q} \cdot \mathbf{r}_j} \right|^2, \quad (7)$$

as shown in Figs. 5(e)–5(h). The intensities of  $S(\mathbf{q})$  near  $(\pm\pi, 0)$  and  $(0, \pm\pi)$  correspond to the fraction of the 2-by-1 domains [Fig. 5(i)], and those near  $(\pm\pi/2, \pm\pi/2)$  correspond to the fraction of the 4-by-4 domains [Fig. 5(j)]. The domain fractions of the 2-by-1 and 4-by-4 orders,  $f(2\text{by}1)$  and  $f(4\text{by}4)$ , are estimated by integrating  $S(\mathbf{q})$  over the circular areas near these  $\mathbf{q}$  values, as shown in Figs. 5(i) and 5(j). Whereas  $\phi(2\text{by}1)$  and  $\phi(4\text{by}4)$  reflect  $S(\mathbf{q})$  only for the  $q$

values corresponding to the uniformly ordered structure,  $f(2\text{by}1)$  and  $f(4\text{by}4)$  integrate  $S(\mathbf{q})$  around the  $q$  values. Because the Fourier transformation of a small domain includes  $S(\mathbf{q})$  around the  $q$  values,  $f(2\text{by}1)$  and  $f(4\text{by}4)$  are considered more suitable for evaluating the fractions of 2-by-1 and 4-by-4 domains in the fine domain structure.  $f(2\text{by}1)$  and  $f(4\text{by}4)$  are found to vary monotonically as a function of  $J_3$  [Fig. 5(k)], reflecting the  $J_3$  dependence of the domain structures, as shown in Figs. 5(a)–5(d).

Having clarified the microscopic structure of the metastable phase, we discuss how the energy barrier found in the simulation can be evaluated on the basis of the microscopic structure. We consider a single spin-flip to break the uniform competing order, which corresponds to Fig. 5(l) for  $J_3 = 0.75 - 1.5$  and to Fig. 5(m) for  $J_3 = 0 - 0.75$ . The energy barrier  $\Delta E_o$  required for these processes is calculated and plotted in Fig. 5(n) and is found to be much larger than  $\Delta_{st}$ . This discrepancy in the energy barrier reflects the fact that the single spin-flips in the uniformly ordered phase are not a direct factor determining the robustness of the metastability. Because the metastable phases that we are discussing are highly disordered and the locally formed order is often surrounded by disordered states, the discrepancy between  $\Delta E_o$  and  $\Delta_{st}$  is rather reasonable. To account for the probability that a locally formed competing order is surrounded by disordered states, the energy barrier is scaled by the domain fraction as  $\Delta E_s = f(4\text{by}4)\Delta E_o$  for

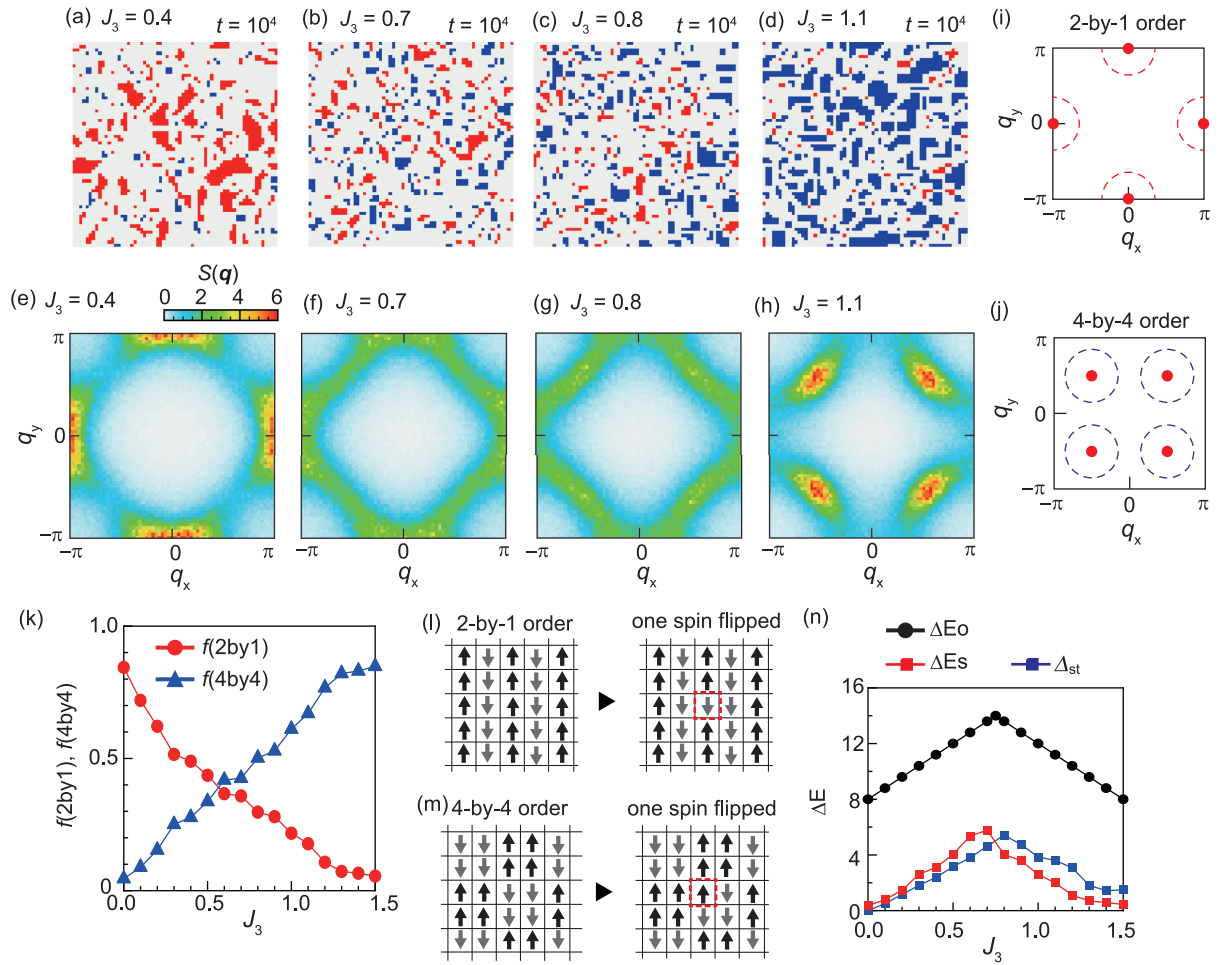


FIG. 5. (a)–(d) Three-colored representation of the spin configurations at  $T = 0.1$  and  $t = 10^4$  for  $J_3 = 0.4$  (a),  $0.7$  (b),  $0.8$  (c), and  $1.1$  (d). (e)–(h) Structure factor  $S(\mathbf{q})$  of the metastable phase shown in panels (a)–(d). (i), (j) Structure factor  $S(\mathbf{q})$  of the uniform 2-by-1 order (i) and 4-by-4 order (j). (k)  $J_3$  dependence of the estimated domain fractions of the 2-by-1 and 4-by-4 orders,  $f(2by1)$  and  $f(4by4)$ . See the main text and Appendix C for details of the estimation method. (l), (m) Single spin-flip process for the uniform 2-by-1 order (l) and 4-by-4 order (m). (n)  $J_3$  dependence of the energy barriers  $\Delta E_o$  and  $\Delta E_s$ .  $\Delta E_o$  is the energy increase due to the single spin-flip processes shown in panel (l) for  $0.75 < J_3 < 1.5$  and panel (m) for  $0 < J_3 < 0.75$ . The scaled energy barrier  $\Delta E_s$  equals  $f(4by4)\Delta E_o$  for  $0 < J_3 < 0.75$  and  $f(2by1)\Delta E_o$  for  $0.75 < J_3 < 1.5$ .

$0 < J_3 < 0.75$  and  $f(2by1)\Delta E_o$  for  $0.75 < J_3 < 1.5$ . We then find that values of  $\Delta E_s$  are close to those of  $\Delta_{st}$  [Fig. 5(n)]. The correspondence between the scaled energy barrier  $\Delta E_s$  and that obtained by the Arrhenius law  $\Delta_{st}$  suggests a method for quantitatively estimating energy barriers from microscopic structures.

## VI. DISCUSSIONS

In the mean-field approximation, the metastable solution of a disordered phase is lost when the system is supercooled below the spinodal point [49]. Similarly, in the present Ising model at  $J = 0.7$ , the local minimum close to  $\phi(2by1) = 0$  is lost at  $T = 2.18$ , which is only a few percent below  $T_c$  [see Fig. 6(c) in Appendix A]. However, the disappearance of a metastable solution does not necessarily indicate the absence of a practically stable phase. Indeed, the present study shows that a practically metastable phase exists even when the system is deeply supercooled. This type of metastability is often observed in solid solutions produced by rapid cooling. For

example, in the  $\text{TiO}_2\text{-VO}_2$  system, spinodal decomposition occurs at temperatures below 830 K, but under rapid cooling, a stable solid solution with a uniform distribution of Ti and V ions can be obtained at room temperature [50], meaning that spinodal decomposition is kinetically arrested. Such kinetic arrest of spinodal decomposition is widely accepted in the context of conserved systems, as the diffusion processes accompanying decomposition reasonably account for the energy barriers responsible for the arrest. In nonconserved systems, however, whether kinetic arrest occurs is nontrivial, since the spinodal growth does not require decomposition, and the energy barriers depend strongly on the underlying interactions of many-body systems. The appearance of a metastable phase in the present Ising model demonstrates that kinetic arrest of spinodal growth can also occur in a nonconserved system, implying the universality of kinetic arrest beyond obvious free-energy minima.

Finally, we discuss the possible relevance of the present simulations for correlated electron materials. Transition metal oxides are typical examples of materials with eutectic-type

geometries in electronic phase diagrams [51–53]. In manganites with a composition in which two electronic phases compete, a glassy electronic state appears under the cooling process with a standard cooling rate due to the effect of randomness [52]. This sensitivity to randomness may indicate a tendency for a metastable disordered phase to appear under thermal quenching. In terms of the energetic competition between multiple ordered phases, geometrical frustration, as in the case of triangular lattices, can also be effective in realizing metastable phases. For example, in quarter-filled triangular lattice systems  $\theta$ -(BEDT-TTF) $_2X$ , several charge-ordered patterns are energetically close to each other, indicating energetic competition [54–57]. Metastable charge glass phases are less likely to appear under a cooling process with a certain cooling rate when the triangular lattice is distorted [12,58], indicating that frustration is effective for inducing metastable phases. Thus, frustrated systems, which have attracted much attention for the exploration of exotic quantum phases, are promising for the realization of metastable electronic phases.

## VII. CONCLUDING REMARKS

The present study aims to generalize the principle of metastability established in metallurgy with the goal of applying it to correlated electron systems. We have demonstrated that a thermally quenched disordered phase exhibits metastability near the eutecticlike triple point in the Ising model with competing interactions. This simple model of metastability enables us to discuss how metastability varies with the interaction strength and how it correlates with local structures. The nature of metastability revealed by the model is likely relevant to experimentally observed metastable electronic phases, suggesting a link to correlated electron systems.

Microscopic simulations address phenomena of a limited time range due to computational constraints. Therefore, the appearance of a metastable phase may simply indicate that the time range is insufficient to reach the most stable phase. In addition, the physics research of correlated electron systems has focused mainly on their most stable phases. Thus, numerically found metastable phases have not received much attention. However, many metastable materials have been created by exploring states before the most stable state is reached. If we focus on the physics of metastability, then a numerically obtained metastable phase would become a valuable research target.

## ACKNOWLEDGMENTS

H.O. thanks H. Ohtani, M. Enoki, K. Nakanishi, and H. Kageyama for fruitful discussions. Calculations were performed using computational resources of the Supercomputer Center at the Institute for Solid State Physics, the University of Tokyo. This work was supported by JST PRESTO (Grant No. JPMJPR21Q2), the Center of Innovation for Sustainable Quantum AI (SQAI), JST (Grant No. JPMJPF2221), JST CREST (Grant No. JPMJCR24I1), and JSPS KAKENHI (Grants No. 22H01164, No. 23K22435, No. 23H04861, No. 22K03508, and No. 24H01609). MANA is supported by World Premier International Research Center Initiative (WPI), MEXT, Japan.

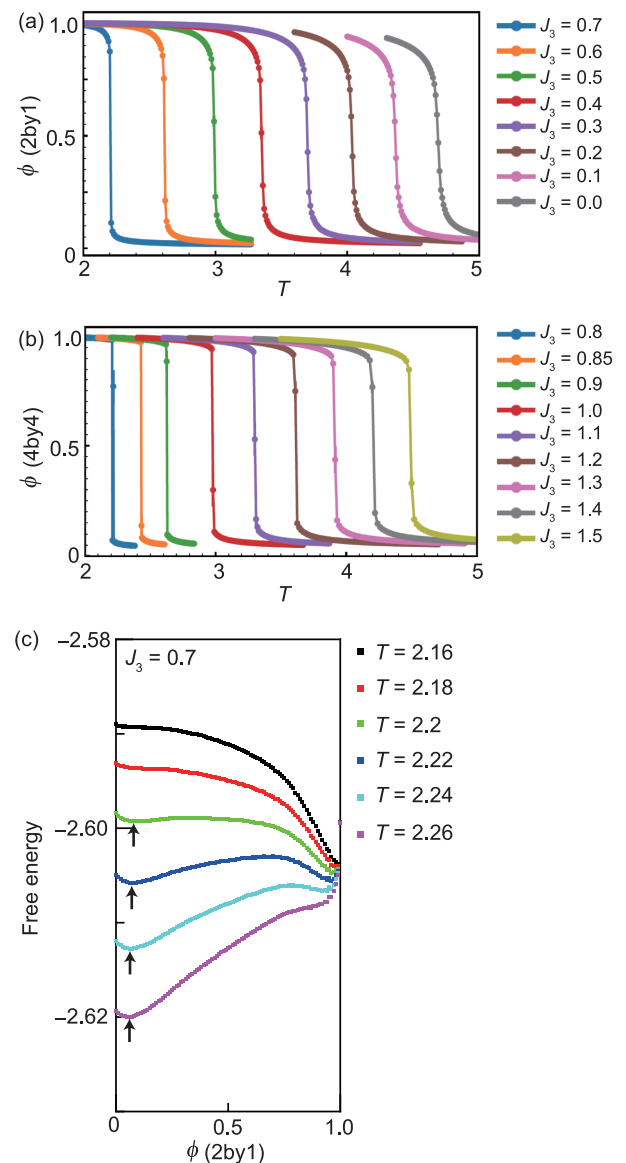


FIG. 6. (a), (b) Temperature dependence of the order parameters  $\phi(2by1)$  for  $J_3 = 0.0 - 0.7$  (a) and  $\phi(4by4)$  for  $J_3 = 0.8 - 1.5$  (b). (c) Free-energy landscape for  $J_3 = 0.7$  near the ordering temperature. The arrows indicate the minimum free energy near  $\phi(2by1) = 0$ .

## DATA AVAILABILITY

The data that support the findings of this article are not publicly available. The data are available from the authors upon reasonable request.

## APPENDIX A

The phase transition temperature of the Ising model was determined from the temperature dependence of the order parameter when the free energy reaches a minimum value (Fig. 6). When  $J_3$  is less than 0.75, a 2-by-1 order forms at the phase transition temperature, whereas when it is greater than 0.75, a 4-by-4 order forms. The order parameter shows a discontinuous change at the phase transition temperature,

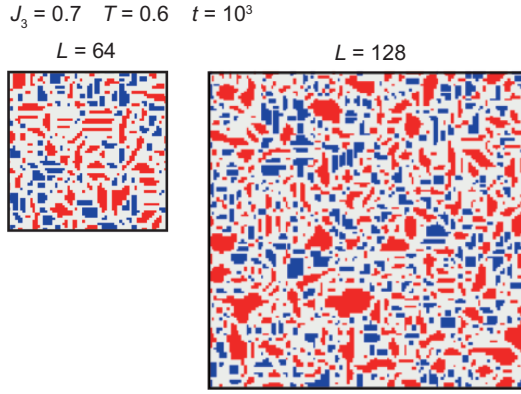


FIG. 7. Spin configurations at parameters of  $(T, J_3) = (0.6, 0.7)$ ,  $t = 10^3$ , and  $L = 64$  and  $128$ .

indicating a first-order phase transition. The free energy was calculated using the Wang-Landau algorithm with the system size  $N = L^2 = 32^2$  [59]. The behavior discussed in Fig. 6(c), in which the local minimum near  $\phi(2\text{by}1) = 0$  disappears between  $T = 2.18$  and  $T = 2.2$ , was also observed for  $L = 24$ . Thus,  $L = 32$  is large enough to reliably capture the temperature dependence of the free-energy minimum. Furthermore, using  $L = 64$ , we confirmed the order-parameter jump at the first-order transition temperature, shown in Figs. 6(a) and 6(b). The temperatures at which the order parameter jumps and at which the minimum point of the free energy shifts in Fig. 6(c) are almost the same, indicating that the size dependence is sufficiently small.

## APPENDIX B

To check the system-size dependence, a comparison between system sizes  $N (= L^2)$  of  $64^2$  and  $128^2$  is shown in Fig. 7. Although the typical domain size is not dependent on the system size, the order parameter is by definition dependent on the system size for the following reasons. The order parameter  $\phi(2\text{by}1)$  can be rewritten as

$$\phi(2\text{by}1) = \sqrt{\frac{1}{N} \left( \sum_{\mathbf{q}=q_x, q_y} S(\mathbf{q}) \right)}, \quad (\text{B1})$$

and the structure factor  $S(\mathbf{q})$  can be rewritten as

$$S(\mathbf{q}) = \frac{1}{N} \sum_{j,k=1}^N \langle \sigma_j \sigma_k \rangle e^{i\mathbf{q} \cdot (\mathbf{r}_j - \mathbf{r}_k)}, \quad (\text{B2})$$

where  $\langle \sigma_j \sigma_k \rangle$  is the correlation function of spins at sites  $j$  and  $k$ .  $\sigma_j \sigma_k e^{i\mathbf{q} \cdot (\mathbf{r}_j - \mathbf{r}_k)}$  is 1 if sites  $i$  and  $j$  are in the same domain of the ordered structure with wave number  $\mathbf{q}$  and can otherwise take a random value whose absolute value is 1. Therefore, the value obtained by taking the sum of this quantity over  $k$  is approximately equal to  $N_q^j$ , which is the domain size of the ordered structure with wave number  $\mathbf{q}$  containing site  $j$ . The structural factor can then be expressed approximately as

$$S(\mathbf{q}) \sim \frac{1}{N} \sum_{j=1}^N \langle N_q^j \rangle. \quad (\text{B3})$$

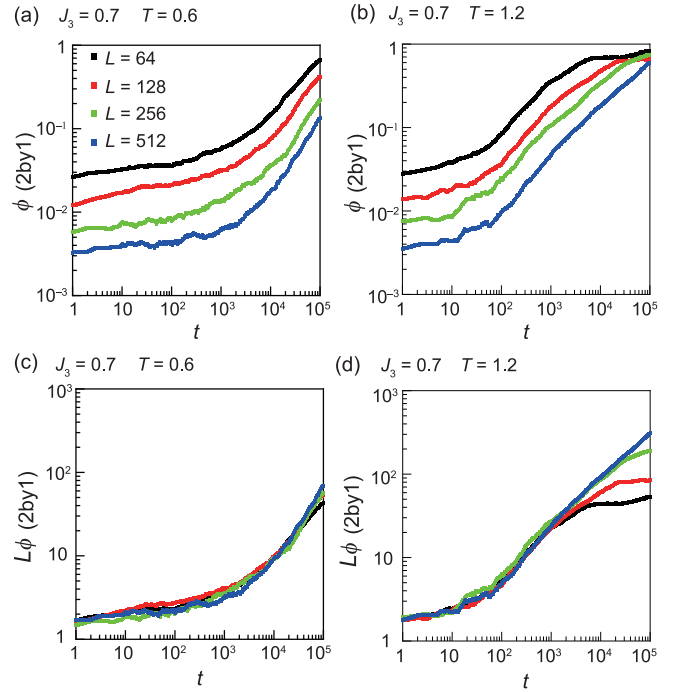


FIG. 8. (a), (b) Isothermal time evolution of  $\phi(2\text{by}1)$  for  $(T, J_3) = (0.6, 0.7)$  (a) and  $(T, J_3) = (0.6, 0.7)$  (b). (c), (d) Isothermal time evolution of  $L\phi(2\text{by}1)$  for  $(T, J_3) = (0.6, 0.7)$  (c) and  $(T, J_3) = (0.6, 0.7)$  (d). The size dependence was examined at  $L = 64, 128, 256$ , and  $512$ .

The domain size and the number of domains are approximately proportional to  $\xi^2$  and  $N/\xi^2$ , respectively, where  $\xi$  is the correlation length. The structure factor can then be approximated by taking the sum over  $j$  as

$$S(\mathbf{q}) \sim \xi^2. \quad (\text{B4})$$

The order parameter is then expressed as

$$\phi(2\text{by}1) \sim \frac{\xi}{L}. \quad (\text{B5})$$

Thus,  $\phi(2\text{by}1)$  depends on the system size when  $\xi$  does not. We observed that  $L\phi(2\text{by}1)$  remains independent of the system size up to the timescale at which  $L\phi(2\text{by}1) \sim \xi$  approaches  $L$  (Fig. 8). When the typical domain size is equal to the system size, the order estimate described above is no longer valid. Therefore, this scaling does not hold when  $\phi(2\text{by}1)$  is close to 1. In the present study, we focus on the dynamics when  $\phi(2\text{by}1)$  is less than 0.5 to discuss the properties that are independent of the system size. In this  $\phi(2\text{by}1)$  range,  $L\phi(2\text{by}1)$  shows similar behavior for  $L = 64, 128, 256$ , and  $512$ , as seen in the TTT diagrams (Fig. 9), so we examined the  $T$ - $J_3$  dependence in detail for  $L = 64$ .

As mentioned above, the present simulations investigate the growth of  $\xi$ . According to previous studies [60,61], scaling analysis of the free energy shows that the bulk term scales as  $L^d$ , while the surface term scales as  $L^{d-1}$ , where  $d$  is the spatial dimension. Drawing an analogy from this scaling analysis, by substituting  $L$  with  $\xi$  and setting  $d = 2$ , the bulk free energy scales as  $N_D \xi^2$ , and the interfacial energy between domains scales as  $N_D \xi$ , where  $N_D$  is the number of stable

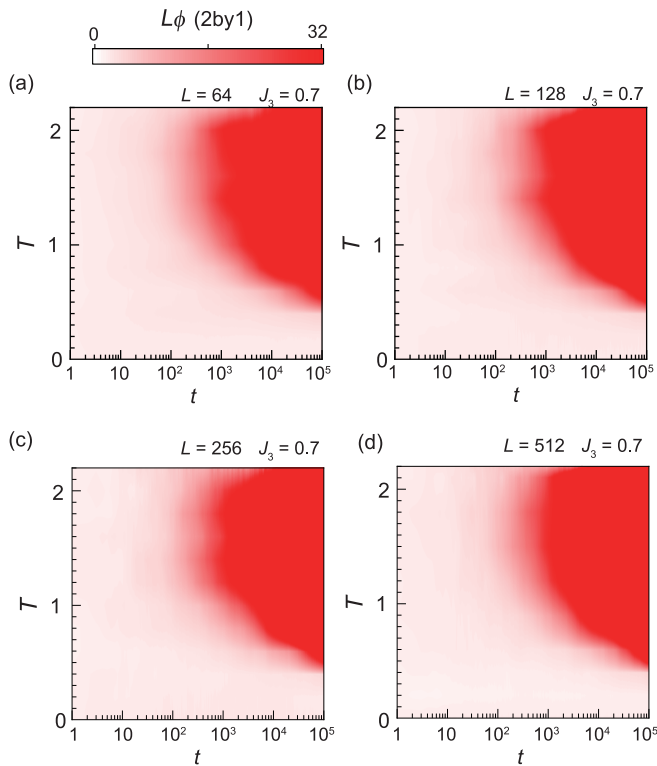


FIG. 9. (a)–(d) TTT diagram plotted based on  $L\phi(2by1)$  for  $J_3 = 0.7$  and  $L = 64$  (a), 128 (b), 256 (c), and 512 (d).

ordered domains. Since  $N_D \sim (L/\xi)^2$ , the bulk and interfacial energy contributions scale as  $L^2$  and  $L^2/\xi$ , respectively.

This scaling analysis suggests that the interfacial free energy decreases monotonically as  $\xi$  increases, while the bulk contribution remains constant. The monotonic decrease of

free energy with increasing  $\xi$  aligns with the monotonic growth of  $\xi$  over time observed in our simulations. However, it does not account for the thermal activation barriers associated with quantities such as  $\Delta_{st}$ ,  $\Delta_{cp}$ ,  $\Delta E_o$ , and  $\Delta E_s$ . Microscopic simulations—such as those analyzing the internal structure of interfaces in our study—can provide valuable insight into these thermal activation barriers.

### APPENDIX C

The fractions of domains of 2-by-1 and 4-by-4 orders in the disordered phase were estimated from the structure factor as follows. In a uniform 2-by-1 ordered state,  $S(\mathbf{q})$  is equal to  $N$  if  $\mathbf{q}$  is either  $(\pi, 0)$  or  $(0, \pi)$ , which are the points indicated in Fig. 4(i), and 0 if  $\mathbf{q}$  is any other value. In a uniform 4-by-4 ordered state,  $S(\mathbf{q})$  is equal to  $N$  if  $\mathbf{q}$  is  $(\pi/2, \pi/2)$ ,  $(\pi/2, -\pi/2)$ ,  $(-\pi/2, \pi/2)$ , or  $(-\pi/2, -\pi/2)$ , which are the points indicated in Fig. 4(j), and 0 if  $\mathbf{q}$  is any other value. When the 2-by-1 and 4-by-4 orders form a domain structure,  $S(\mathbf{q})$  takes a finite value around the values of  $\mathbf{q}$  corresponding to the 2-by-1 and 4-by-4 orders. The values obtained by integrating the  $S(\mathbf{q})$  of these diffuse spots over the  $\mathbf{q}$  range shown in Figs. 4(i) and 4(j) indicates how much area the 2-by-1 and 4-by-4 domains occupy. Therefore, by normalizing these values by  $N$ , the domain fractions of the 2-by-1 and 4-by-4 orders are estimated as

$$f(2by1) = \frac{1}{N} \sum_{\mathbf{q} \sim \mathbf{q}_x, \mathbf{q}_y} S(\mathbf{q}), \quad (C1)$$

$$f(4by4) = \frac{1}{N} \sum_{\mathbf{q} \sim \mathbf{q}_p, \mathbf{q}_m, -\mathbf{q}_p, -\mathbf{q}_m} S(\mathbf{q}). \quad (C2)$$

- [1] B. Derjaguin, D. Fedoseev, V. Varnin, and S. Vnukov, The nature of metastable phases of carbon, *Nature (London)* **269**, 398 (1977).
- [2] W. Sun, S. T. Dacek, S. P. Ong, G. Hautier, A. Jain, W. D. Richards, A. C. Gamst, K. A. Persson, and G. Ceder, The thermodynamic scale of inorganic crystalline metastability, *Sci. Adv.* **2**, e1600225 (2016).
- [3] W. Sun, A. Holder, B. Orvañanos, E. Arca, A. Zakutayev, S. Lany, and G. Ceder, Thermodynamic routes to novel metastable nitrogen-rich nitrides, *Chem. Mater.* **29**, 6936 (2017).
- [4] A. J. Martinolich and J. R. Neilson, Toward reaction-by-design: achieving kinetic control of solid state chemistry with metathesis, *Chem. Mater.* **29**, 479 (2017).
- [5] M. Bykov, S. Chariton, H. Fei, T. Fedotenko, G. Aprilis, A. V. Ponomareva, F. Tasnádi, I. A. Abrikosov, B. Merle, P. Feldner *et al.*, High-pressure synthesis of ultraincompressible hard rhenium nitride pernitride  $\text{Re}_2(\text{N}_2)(\text{N})_2$  stable at ambient conditions, *Nat. Commun.* **10**, 2994 (2019).
- [6] H. Ito, Y. Nakahira, N. Ishimatsu, Y. Goto, A. Yamashita, Y. Mizuguchi, C. Moriyoshi, T. Toyao, K.-I. Shimizu, H. Oike *et al.*, Stability and metastability of  $\text{Li}_3\text{YCl}_6$  and  $\text{Li}_3\text{HoCl}_6$ , *Bull. Chem. Soc. Jpn.* **96**, 1262 (2023).
- [7] D. Uhlmann, A kinetic treatment of glass formation, *J. Non-Cryst. Solids* **7**, 337 (1972).
- [8] A. L. Greer, Metallic glasses, *Science* **267**, 1947 (1995).
- [9] C. A. Angell, Formation of glasses from liquids and biopolymers, *Science* **267**, 1924 (1995).
- [10] P. G. Debenedetti and F. H. Stillinger, Supercooled liquids and the glass transition, *Nature (London)* **410**, 259 (2001).
- [11] F. Kagawa, T. Sato, K. Miyagawa, K. Kanoda, Y. Tokura, K. Kobayashi, R. Kumai, and Y. Murakami, Charge-cluster glass in an organic conductor, *Nat. Phys.* **9**, 419 (2013).
- [12] H. Oike, F. Kagawa, N. Ogawa, A. Ueda, H. Mori, M. Kawasaki, and Y. Tokura, Phase-change memory function of correlated electrons in organic conductors, *Phys. Rev. B* **91**, 041101(R) (2015).
- [13] S. Sasaki, K. Hashimoto, R. Kobayashi, K. Itoh, S. Iguchi, Y. Nishio, Y. Ikemoto, T. Moriwaki, N. Yoneyama, M. Watanabe *et al.*, Crystallization and vitrification of electrons in a glass-forming charge liquid, *Science* **357**, 1381 (2017).
- [14] M. Yoshida, Y. Zhang, J. Ye, R. Suzuki, Y. Imai, S. Kimura, A. Fujiwara, and Y. Iwasa, Controlling charge-density-wave states in nano-thick crystals of 1T-TiSe<sub>2</sub>, *Sci. Rep.* **4**, 7302 (2014).

- [15] H. Oike, A. Kikkawa, N. Kanazawa, Y. Taguchi, M. Kawasaki, Y. Tokura, and F. Kagawa, Interplay between topological and thermodynamic stability in a metastable magnetic skyrmion lattice, *Nat. Phys.* **12**, 62 (2016).
- [16] G. Berruto, I. Madan, Y. Murooka, G. M. Vanacore, E. Pomarico, J. Rajeswari, R. Lamb, P. Huang, A. J. Kruchkov, Y. Togawa, T. LaGrange, D. McGrouther, H. M. Rønnow, and F. Carbone, Laser-induced skyrmion writing and erasing in an ultrafast cryo-Lorentz transmission electron microscope, *Phys. Rev. Lett.* **120**, 117201 (2018).
- [17] X. Yu, D. Morikawa, T. Yokouchi, K. Shibata, N. Kanazawa, F. Kagawa, T.-H. Arima, and Y. Tokura, Aggregation and collapse of skyrmions in a non-equilibrium state, *Nat. Phys.* **14**, 832 (2018).
- [18] M. T. Birch, R. Takagi, S. Seki, M. N. Wilson, F. Kagawa, A. Štefančič, G. Balakrishnan, R. Fan, P. Steadman, C. J. Ottley, M. Crisanti, R. Cubitt, T. Lancaster, Y. Tokura, and P. D. Hatton, Increased lifetime of metastable skyrmions by controlled doping, *Phys. Rev. B* **100**, 014425 (2019).
- [19] T. Katsufuji, T. Kajita, S. Yano, Y. Katayama, and K. Ueno, Nucleation and growth of orbital ordering, *Nat. Commun.* **11**, 2324 (2020).
- [20] K. Matsuura, H. Oike, V. Kocsis, T. Sato, Y. Tomioka, Y. Kaneko, M. Nakamura, Y. Taguchi, M. Kawasaki, Y. Tokura *et al.*, Kinetic pathway facilitated by a phase competition to achieve a metastable electronic phase, *Phys. Rev. B* **103**, L041106 (2021).
- [21] K. Matsuura, Y. Nishizawa, M. Kriener, T. Kurumaji, H. Oike, Y. Tokura, and F. Kagawa, Thermodynamic determination of the equilibrium first-order phase-transition line hidden by hysteresis in a phase diagram, *Sci. Rep.* **13**, 6876 (2023).
- [22] H. Oike, M. Kamitani, Y. Tokura, and F. Kagawa, Kinetic approach to superconductivity hidden behind a competing order, *Sci. Adv.* **4**, eaau3489 (2018).
- [23] L. Stojchevska, I. Vaskivskiy, T. Mertelj, P. Kusar, D. Svetin, S. Brazovskii, and D. Mihailovic, Ultrafast switching to a stable hidden quantum state in an electronic crystal, *Science* **344**, 177 (2014).
- [24] I. Vaskivskiy, J. Gospodaric, S. Brazovskii, D. Svetin, P. Sutar, E. Goresnik, I. A. Mihailovic, T. Mertelj, and D. Mihailovic, Controlling the metal-to-insulator relaxation of the metastable hidden quantum state in 1T-TaS<sub>2</sub>, *Sci. Adv.* **1**, e1500168 (2015).
- [25] V. Molinero, S. Sastry, and C. A. Angell, Tuning of tetrahedrality in a silicon potential yields a series of monatomic (metal-like) glass formers of very high fragility, *Phys. Rev. Lett.* **97**, 075701 (2006).
- [26] M. Kobayashi and H. Tanaka, Possible link of the V-shaped phase diagram to the glass-forming ability and fragility in a water-salt mixture, *Phys. Rev. Lett.* **106**, 125703 (2011).
- [27] Y. Waseda and K. Suzuki, Structure of molten silicon and germanium by X-ray diffraction, *Z. Phys. B* **20**, 339 (1975).
- [28] T. A. Weber and F. H. Stillinger, Local order and structural transitions in amorphous metal-metalloid alloys, *Phys. Rev. B* **31**, 1954 (1985).
- [29] H. Tanaka, Relationship among glass-forming ability, fragility, and short-range bond ordering of liquids, *J. Non-Cryst. Solids* **351**, 678 (2005).
- [30] H. Tanaka, Possible resolution of the Kauzmann paradox in supercooled liquids, *Phys. Rev. E* **68**, 011505 (2003).
- [31] T.-D. Lee and C.-N. Yang, Statistical theory of equations of state and phase transitions. II. Lattice gas and Ising model, *Phys. Rev.* **87**, 410 (1952).
- [32] C. Van Baal, Order-disorder transformations in a generalized Ising alloy, *Physica* **64**, 571 (1973).
- [33] G. F. Newell and E. W. Montroll, On the theory of the Ising model of ferromagnetism, *Rev. Mod. Phys.* **25**, 353 (1953).
- [34] C. Castellani, C. Di Castro, D. Feinberg, and J. Ranninger, New model Hamiltonian for the metal-insulator transition, *Phys. Rev. Lett.* **43**, 1957 (1979).
- [35] P. Fratzl and O. Penrose, Kinetics of spinodal decomposition in the Ising model with vacancy diffusion, *Phys. Rev. B* **50**, 3477 (1994).
- [36] P. Fratzl, O. Penrose, R. Weinkamer, and I. Žižak, Coarsening in the Ising model with vacancy dynamics, *Phys. A (Amsterdam, Neth.)* **279**, 100 (2000).
- [37] P. A. Rikvold, H. Tomita, S. Miyashita, and S. W. Sides, Metastable lifetimes in a kinetic Ising model: Dependence on field and system size, *Phys. Rev. E* **49**, 5080 (1994).
- [38] P. A. Rikvold, G. Brown, S. Miyashita, C. Omand, and M. Nishino, Equilibrium, metastability, and hysteresis in a model spin-crossover material with nearest-neighbor antiferromagnetic-like and long-range ferromagnetic-like interactions, *Phys. Rev. B* **93**, 064109 (2016).
- [39] A. Lipowski and D. Johnston, Metastability in a four-spin Ising model, *J. Phys. A: Math. Gen.* **33**, 4451 (2000).
- [40] A. Lipowski and D. Johnston, Crystallization of a supercooled liquid and of a glass: Ising model approach, *Phys. Rev. E* **64**, 041605 (2001).
- [41] P. Dimopoulos, D. Espriu, E. Jané, and A. Prats, Slow dynamics in the three-dimensional gonihedric model, *Phys. Rev. E* **66**, 056112 (2002).
- [42] G. Savvidy, The gonihedric paradigm extension of the Ising model, *Mod. Phys. Lett. B* **29**, 1550203 (2015).
- [43] D. Landau and K. Binder, Phase diagrams and critical behavior of Ising square lattices with nearest-, next-nearest-, and third-nearest-neighbor couplings, *Phys. Rev. B* **31**, 5946 (1985).
- [44] D. Thouless, Exchange in solid <sup>3</sup>He and the Heisenberg Hamiltonian, *Proc. Phys. Soc.* **86**, 893 (1965).
- [45] G. Misguich, C. Lhuillier, B. Bernu, and C. Waldtmann, Spin-liquid phase of the multiple-spin exchange Hamiltonian on the triangular lattice, *Phys. Rev. B* **60**, 1064 (1999).
- [46] A. J. Bray, Theory of phase-ordering kinetics, *Adv. Phys.* **43**, 357 (1994).
- [47] M. Naskar, M. Acharyya, E. Vatansever, and N. G. Fytas, Metastable behavior of the spin-*s* Ising and Blume-Capel ferromagnets: A Monte Carlo study, *Phys. Rev. E* **104**, 014107 (2021).
- [48] T. Sato, K. Miyagawa, and K. Kanoda, Electronic crystal growth, *Science* **357**, 1378 (2017).
- [49] S. Miyashita, *Collapse of Metastability* (Springer, Berlin, 2022), pp. 28–30.
- [50] Z. Hiroi, H. Hayamizu, T. Yoshida, Y. Muraoka, Y. Okamoto, J.-I. Yamaura, and Y. Ueda, Spinodal decomposition in the TiO<sub>2</sub>-VO<sub>2</sub> system, *Chem. Mater.* **25**, 2202 (2013).
- [51] Y. Tokura and Y. Tomioka, Colossal magnetoresistive manganites, *J. Magn. Mater.* **200**, 1 (1999).
- [52] Y. Tokura, Critical features of colossal magnetoresistive manganites, *Rep. Prog. Phys.* **69**, 797 (2006).

- [53] K. Shibuya, M. Kawasaki, and Y. Tokura, Metal-insulator transition in  $V_{1-x}W_xO_2$  ( $\leq x \leq 0.33$ ) epitaxial thin films epitaxial thin films, *Appl. Phys. Lett.* **96**, 022102 (2010).
- [54] H. Seo, Charge ordering in organic ET compounds, *J. Phys. Soc. Jpn.* **69**, 805 (2000).
- [55] Y. Pramudya, H. Terletska, S. Pankov, E. Manousakis, and V. Dobrosavljević, Nearly frozen Coulomb liquids, *Phys. Rev. B* **84**, 125120 (2011).
- [56] S. Mahmoudian, L. Rademaker, A. Ralko, S. Fratini, and V. Dobrosavljević, Glassy dynamics in geometrically frustrated Coulomb liquids without disorder, *Phys. Rev. Lett.* **115**, 025701 (2015).
- [57] L. Rademaker, Z. Nussinov, L. Balents, and V. Dobrosavljević, Suppressed density of states in self-generated Coulomb glasses, *New J. Phys.* **20**, 043026 (2018).
- [58] T. Sato, F. Kagawa, K. Kobayashi, A. Ueda, H. Mori, K. Miyagawa, K. Kanoda, R. Kumai, Y. Murakami, and Y. Tokura, Systematic variations in the charge-glass-forming ability of geometrically frustrated  $\theta$ -(BEDT-TTF) $_2X$  organic conductors, *J. Phys. Soc. Jpn.* **83**, 083602 (2014).
- [59] F. Wang and D. P. Landau, Determining the density of states for classical statistical models: A random walk algorithm to produce a flat histogram, *Phys. Rev. E* **64**, 056101 (2001).
- [60] J. Lee and J. M. Kosterlitz, New numerical method to study phase transitions, *Phys. Rev. Lett.* **65**, 137 (1990).
- [61] J. Lee and J. M. Kosterlitz, Finite-size scaling and Monte Carlo simulations of first-order phase transitions, *Phys. Rev. B* **43**, 3265 (1991).